Impact of disintegrants on rheological properties and printability in SSE 3D printing of immediate-release formulations

Morenikeji Aina, Darya Kuznyetsova, Fabien Baillon, Romain Sescousse, Noelia M. Sanchez-Ballester, Sylvie Begu, Ian Soulairol, Martial Sauceau

European Journal of Pharmaceutical Sciences 206 (2025) 107017

Contents lists available at ScienceDirect

European Journal of Pharmaceutical Sciences

journal homepage: www.elsevier.com/locate/ejps

Impact of disintegrants on rheological properties and printability in SSE 3D printing of immediate-release formulations

Morenikeji Aina [a,*], Darya Kuznyetsova [a], Fabien Baillon [a], Romain Sescousse [a], Noelia M. Sanchez-Ballester [b,c], Sylvie Begu [b], Ian Soulairol [b,c], Martial Sauceau [a]

[a] RAPSODEE, IMT Mines Albi, CNRS, University of Toulouse, 81013 Albi, France
[b] ICGM, University of Montpellier, CNRS, ENSCM, Montpellier, France
[c] Department of Pharmacy, Nîmes University Hospital, Nîmes, France

ARTICLE INFO

Dataset link: Recherche Data Gouv

Keywords:
Personalised medicine
Disintegrant
3D printing
Semi-solid extrusion (SSE)
Immediate release
Printability
Rheology

ABSTRACT

This study investigates the effects of disintegrants sodium starch glycolate (SSG) and crospovidone (CP) on the printability, rheological properties, and disintegration time of agar and hydroxypropyl methylcellulose (HPMC)-based formulations designed for semi-solid extrusion. Printability was assessed by measuring the dimensional accuracy of manually extruded filaments. Rheological analysis was performed using oscillatory measurements. Principal component analysis (PCA) and Spearman correlation analysis identified three key components (phase angle, critical strain, and elastic modulus) that explained the total variance in the rheological dataset. A 2×3^2 factorial design was employed to evaluate the impact of CP, SSG, and HPMC on these rheological parameters, as well as on printability and disintegration time. Results indicated that formulations containing HPMC and SSG generally exhibited better printability. Formulations containing CP achieved satisfactory printability only when SSG or HPMC was included. The optimal printability and rheological properties were achieved with formulations containing 5 % CP and 10 % SSG. Linear regression models correlated geometric volumes of the model and pycnometric volumes of printed objects, with validation showing that predicted masses were within a 95 % confidence interval of measured values for various shapes. All formulations demonstrated immediate-release properties, confirming the successful fabrication of personalised immediate-release dosage forms using semi-solid extrusion technology.

1. Introduction

Oral solid dosage forms are the most commonly used form of drug administration. These forms include tablets, capsules, and powders, which offer advantages such as ease of administration, precise dosing, stability, and cost-effectiveness in manufacturing and packaging (Awad et al., 2021; Sohail Arshad et al., 2021). Immediate-release (IR) dosage forms, a type of oral solid dosage form, are particularly favoured due to their rapid dissolution and quick absorption into the bloodstream, leading to prompt therapeutic effects. This swift onset of action makes IR dosage forms suitable for medications that require rapid relief, such as analgesics, antipyretics, and certain cardiovascular drugs (Funk et al., 2022; Steffens and Wagner, 2021; Schick et al., 2020). Furthermore, dispersible tablets (a form of IR dosage form) can be dissolved in water, enhancing the ease of administration for patients who have difficulty swallowing traditional tablets, including children, the elderly, and those with dysphagia (Panraksa et al., 2022; Baral et al., 2021).

However, the current procedure for producing such tablets involves direct compression, where excipients and the active pharmaceutical ingredient (API) are blended before tabletting. This method relies extensively on the flowability and compressibility of the excipients to achieve tablets of uniform weight, ensuring precise drug dosing (Trisopon et al., 2020, 2021). Furthermore, variations in particle sizes between the API and the excipients can cause uneven distribution within the blend. This non-uniform distribution may impact the consistency and efficacy of the final dosage units, highlighting the need for meticulous control over formulation and blending processes. As such, complicated downstream processes such as granulation, blending, compression, and coating are usually carried out (Wilkins et al., 2024; Kokott et al., 2021; Wang et al., 2022). Despite these additional steps, achieving adequate homogeneity is not always guaranteed. For instance, the blending must be meticulously monitored to prevent segregation of the powder mixture, where this segregation can lead to inconsistent drug content in the final tablets, impacting their efficacy and safety (Bowler et al., 2020;

* Corresponding author.
E-mail address: morenikeji.aina@mines-albi.fr (M. Aina).

https://doi.org/10.1016/j.ejps.2025.107017
Received 11 September 2024; Received in revised form 12 November 2024; Accepted 15 January 2025
Available online 21 January 2025

Stranzinger et al., 2021; Rosas et al., 2023).

In contrast, 3D printing (3DP), also known as additive manufacturing, offers a flexible and efficient method for producing immediate-release (IR) dosage forms through layer-by-layer deposition directly from digital designs. Unlike traditional manufacturing processes, 3DP eliminates many intermediate steps, providing precise control over drug release properties. This approach facilitates rapid prototyping, customisation, on-demand manufacturing, and the creation of complex dosage forms (Wang et al., 2022; Liang et al., 2019; Zhang et al., 2018; Abdella et al., 2024). Several 3DP techniques are used to fabricate IR dosage forms, including inkjet printing, stereolithography, selective laser sintering, fused deposition modelling, direct powder extrusion, and semi-solid extrusion (SSE) (Xue et al., 2023; Deon et al., 2022). Among these, SSE has attracted significant attention due to its simplicity and ability to create unique solid dosage forms, such as chewable and gummy tablets (Herrada-Manchón et al., 2020; Tagami et al., 2021). Additionally, SSE does not require high heat, minimising the risk of drug degradation and allowing for a broader range of excipients (El Aita et al., 2020).

Moreover, in the context of *in vitro* drug release or dissolution of these IR dosage forms, excipients play a critical role in facilitating the disintegration of the matrix upon contact with water. This disintegration leads to the fragmentation of the tablet into smaller particles, which is essential for the rapid release of the active pharmaceutical ingredient (API). The disintegration process is often enhanced by the inclusion of disintegrants, which can be either natural or chemically modified (superdisintegrants). Examples of natural disintegrants include starch- and cellulose-based excipients, while commonly used synthetic disintegrants include crospovidone, sodium starch glycolate, and sodium croscarmellose (Funk et al., 2022; Steffens and Wagner, 2021). These disintegrants, particularly superdisintegrants, enhance the disintegration rate, which is vital for the immediate-release properties of the tablet. Although they are widely used, disintegrants and superdisintegrants exhibit different behaviours due to variations in their physicochemical properties and disintegration mechanisms (Berardi et al., 2022; Zarmpi et al., 2017; Berardi et al., 2021). Such differences can introduce challenges related to printability and rheological properties, which are critical for the success of SSE 3DP. Although higher concentrations of disintegrants in SSE 3D printing have been reported compared to traditional tabletting methods (Patel et al., 2021; Roche et al., 2023), research on how disintegrants impact the rheology and printability of SSE formulations remains limited.

In light of this research gap, this study investigates the impact of two widely used pharmaceutical superdisintegrants — crospovidone (CP) and sodium starch glycolate (SSG) — on the disintegration time, rheological properties, and printability of IR formulations intended for SSE 3D printing. This work also aims demonstrate that the incorporation of disintegrant in the formulation would not only accelerate the rate of disintegration, but also enhance the immediate-release properties. To test this hypothesis, we used a previously developed formulation by Aina et al. (2024c), consisting of 3% agar (A), 2% hydroxypropyl methylcellulose (HPMC or H), 10% sucrose (S), and 2 % caffeine (C), was used as a basis. Specifically, it was postulated that formulations with rheological properties similar to those of this previously optimised formulation would also exhibit optimal printability. A 2×3^2 factorial design was employed, considering the mass fractions of HPMC (at 2 levels), CP (at 3 levels), and SSG (at 3 levels). By investigating how CP and SSG influence these key factors, this study aims to contribute to the advancement of fast-disintegrating dosage forms produced using SSE.

2. Materials & methods

2.1. Materials

Agar (Molecular weight, MW = 372.3 g/mol), anhydrous caffeine ($C_8H_{10}N_4O_2$, MW = 194.19 g/mol), and pulverised sucrose ($C_{12}H_{22}O_{11}$, MW = 342.3 g/mol) were purchased from Cooper's Laboratory, France. Methocel® K4M (HPMC, USP 2208 grade, 4000 cp, MW = 2.1×10^5 g/mol, 8.1% hydroxypropyl and 22% methoxy substituted) was a gift from Colorcon Ltd, France. Free samples of Crospovidone and Sodium Starch Glycolate were obtained from JRS Pharma, Germany. Ultrapure water for sample preparation was obtained from a Purelab® water purification system (VWR, France), with a resistance of 18 MΩ cm. All solutions were filtered through a 0.45 μm membrane filter (Merck, France) prior to use.

Table 1
Independent variables in 2×3^2 full factorial design.

Independent variable, factor	Levels used		
	Low (% w/w)	Middle (% w/w)	High (% w/w)
X_1: CP	0	5	10
X_2: SSG	0	5	10
X_3: HPMC (H)	0	–	2

2.2. Preparation of the formulations

As described in a previous study (Aina et al., 2024c), hydrogels containing disintegrants were prepared by mixing A, H, S, C, CP, and SSG in deionised water. Based on their concentrations, the powders were weighed and placed in a beaker, then homogenised using a laboratory spatula. Then, deionised water heated to 98 °C was added to the powder mixture while stirring vigorously. In the case of very viscous samples, a homogeniser (Jankel & Kunkel, Germany) was used to ensure a lump-free paste. The beaker containing the paste was then placed in a water bath at 95 °C for 20 min to maximise the solubilisation of the components. The resulting paste was white when CP or SSG was added, and amber-coloured when HPMC was included. The paste was then left at room temperature (20 °C) overnight before proceeding with rheological analysis and 3D printing.

2.3. Experimental design

A two factor three levels and one factor two levels (2×3^2) full factorial design was used to optimise the rheological properties, printability and disintegration time of hydrogels containing A, S and C. In this study, A was not used as a factor because, based on preliminary studies, it had no significant impact on the disintegration time of formulations. As shown in Table 1, HPMC, CP and SSG were chosen as factors at two, three, and three levels, respectively. The notations for the 18 formulations used, which correspond to the different combinations of the factors and their levels, are listed in Table 2 for reference.

In this context, the factorial design was chosen for its simplicity and efficiency in evaluating the main effects and interactions of the factors. While a Central Composite Design (CCD) can model quadratic effects and higher-order interactions, this was not necessary for this study, which primarily focused on assessing the effects of the key factors without the added complexity of higher-order modelling. Additionally, the factor levels were carefully selected to ensure significant responses while keeping the formulation practical. In future studies requiring more detailed optimisation, a CCD could be used to explore higher-order interactions and further refine the formulation.

2.4. Printability assessment

One limitation of the semi-quantitative printability assessment method developed by Ouyang et al. (2016) was the need to use a 3D printer for the evaluation. For a 3D printer requiring 200–300 g per printing, this could lead to the wastage of excess feedstock. In this study, a printability test was conducted by manually extruding the material from a syringe to replicate the printing process. To minimise

Table 2
Samples for the experimental design: notation and aqueous composition (in % w/w).

Notation	Agar, A	HPMC, H	Sucrose, S	Caffeine, C	Crospovidone, CP	Sodium starch glycolate, SSG
0CP0SSG	3	–	10	2	–	–
5CP0SSG	3	–	10	2	5	–
10CP0SSG	3	–	10	2	10	–
0CP5SSG	3	–	10	2	–	5
0CP10SSG	3	–	10	2	–	10
5CP5SSG	3	–	10	2	5	5
5CP10SSG	3	–	10	2	5	10
10CP5SSG	3	–	10	2	10	5
10CP10SSG	3	–	10	2	10	10
2H0CP0SSG	3	2	10	2	–	–
2H5CP0SSG	3	2	10	2	5	–
2H10CP0SSG	3	2	10	2	10	–
2H0CP5SSG	3	2	10	2	–	5
2H0CP10SSG	3	2	10	2	–	10
2H5CP5SSG	3	2	10	2	5	5
2H5CP10SSG	3	2	10	2	5	10
2H10CP5SSG	3		10	2	10	5
2H10CP10SSG	3	2	10	2	10	10

Table 3
Sample notation and aqueous composition (in % w/w).

Notation	Agar, A	HPMC, H	Sucrose, S	Caffeine, C
3A	3	–	–	–
3A2H	3	2	–	–
3A3H	3	3	–	–
3A4H	3	4	–	–
3A5H	3	5	–	–
4A	4	–	–	–
4A2H	4	2	–	–
4A3H	4	3	–	–
4A4H	4	4	–	–
4A5H	4	5	–	–
10S0C	3	2	10	0
10S1C	3	2	10	1
10S2C	3	2	10	2
10S3C	3	2	10	3
10S5C	3	2	10	5
10S7C	3	2	10	7
10S10C	3	2	10	10

operator influence, two individuals performed the test. Formulations similar to those from a previous study (Table 3) were prepared, and the results from the manual syringe test were compared with those obtained from a 3D printer (Aina et al., 2024c). This comparison aimed to assess the effectiveness of the manual syringe test for evaluating the printability of the formulations containing disintegrants.

To determine printability (Pr, unitless), extrudates from a syringe were used to trace 1.6 × 1.6 cm square grids printed on paper. Photos of these extrudates were analysed using ImageJ to measure their perimeter (L) and area (A) (n = 4). The Pr was calculated using the formula in Eq. (1). In ideal conditions, a Pr value of 1 indicates optimal gelation, demonstrating excellent extrudability and shape retention properties. Values lower than 1 (Pr < 1) suggest under-gelled formulations, which exhibit poor shape retention but better extrudability. Conversely, values greater than 1 (Pr > 1) indicate over-gelled formulations, leading to irregular filaments with fractured morphology and poor extrudability; however, these samples tend to exhibit good shape retention. For extrusion purposes, Pr values between 0.9 and 1.1 are generally considered indicative of good gelation (Ouyang et al., 2016). In this study, the range for good printability was defined as between 0.94 and 1.14, which aligns with the range established in a previous study (Aina et al., 2024c). In that study, samples below this range exhibited poor shape fidelity, while those above this range showed poor extrudability.

$$Pr = \frac{L^2}{16A} \quad (1)$$

2.5. Rheological characterisation

Unlike our previous study (Aina et al., 2024c), this study focused solely on oscillatory measurements. This decision was made based on three key reasons: (1) oscillatory measurements have been shown to be sufficient for characterising rheological properties (Aina et al., 2024c); (2) the shear rate regime of rotational rheometers is lower than that encountered during 3D printing, making rotational measurements less effective at describing the material's flow properties during printing (Aina et al., 2024a); and (3) the torque required to measure the flow properties of some pastes exceeded the capacity of the rotational rheometer. Thus, only the information regarding the viscoelastic properties of the disintegrant-containing paste was obtained. In addition, rheological analysis could not be performed for 5CP0SSG and 10CP0SSG due to the difficulty in placing homogeneous samples between the plates. These samples were therefore excluded from the rheological study.

The linear viscoelastic region (LVER) was first located under controlled stress mode. Subsequently, the plateau values of the elastic or storage modulus (G' in Pa), viscous or loss modulus (G'') and phase angle (δ in °) were obtained in the LVER of the oscillation sweep from 1–1000 Pa at 1 Hz. Furthermore, the exponent (m, dimensionless) was obtained from the fit of the G' and the frequency, f (1–10 Hz) at 30 Pa (within the LVER) to a power law equation. However, the critical strain (γ_c, %) and elastic limit or critical stress (τ_c, Pa) were defined as the strain and stress, respectively at the end of the LVER (where the G' deviated ±10% from the plateau value). Also, the change in elastic modulus (CEM) was defined as the difference between the G' at the end of the LVER and the G' at the end of the analysis (at 1000 Pa). All measurements were performed in duplicates at 20 °C.

2.6. Disintegration time

Apart from possessing good printability, the choice of the optimum formulation was based on the disintegration time. Therefore, as a preliminary step, round objects (n = 3) of about 1.2 g were manually extruded. The disintegration times of the manually fabricated circles were assessed using a tablet disintegration tester (DT50, Sotax AG, Switzerland) with 500 ml of ultrapure water. The test was conducted at 37 ±0.5 °C. Objects that disintegrated within 3 min were assigned 1 whereas those that did not were assigned 2.

2.7. Printing process

An optimal formulation was selected based on a comprehensive assessment of the formulation's rheological properties, the printability

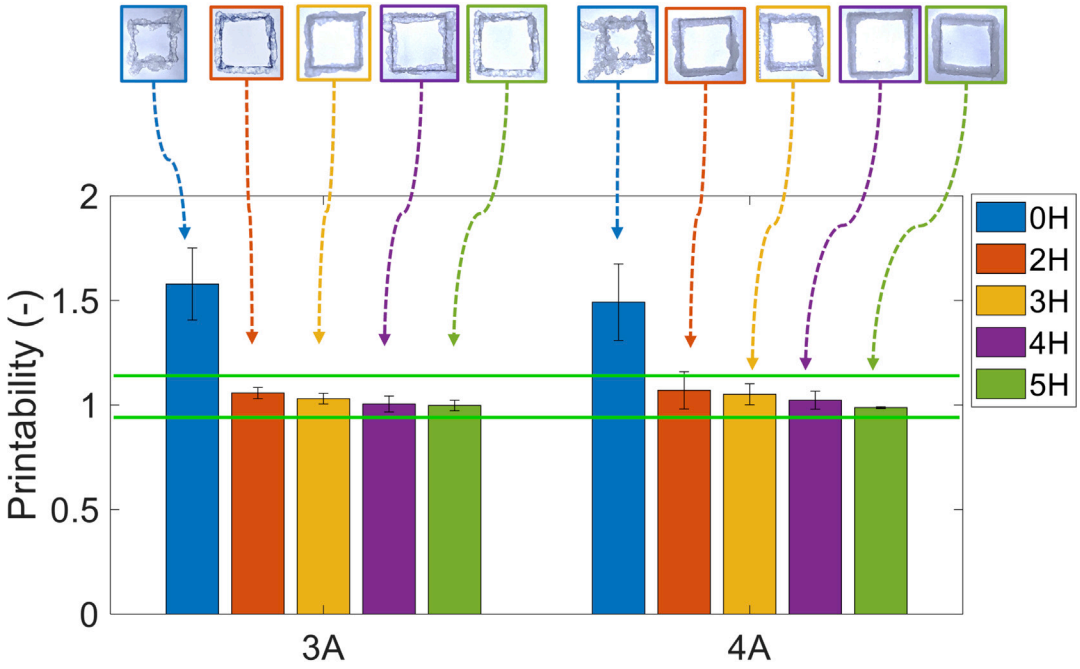

Fig. 1. Printability values of A and AH gels. Error bars are standard deviations based on four replicates.

Table 4
Dimensions of the models printed.

Shape	d_1 (mm)	d_2 (mm)	h (mm)
Cylinder	5.3	5.3	3.6
Heart	12	12	4.8
Oblong	12	6	4

of the manually extruded samples, and the disintegration properties of the manually fabricated objects. Using this optimal formulation, SSE 3DP was performed using a Delta WASP 2040 printer equipped with the clay module (WASP, Italy) at room temperature. The layer height of each object was set to 0.4 mm, the infill pattern was rectilinear at an infill density of 100%. The nozzle diameter used in this study was 0.84 mm at a print head speed of 20 mm/s. The dimensions of the models printed, including d_1 (the diameter of the base), d_2 (the diameter of the top), and h (the height), are shown in Table 4.

The geometrical volumes of the models were obtained by calculating the volume of the cylindrical, oblong and heart-shaped model (Eqs. (2) and (3)). The volume of the printed samples (n = 2) were measured using an AccuPyc™ 1330 (Micromeritics, France) gas pycnometer. Tablets' weights were recorded after printing using an analytical balance (Sartorius™ BCE224I-1S, France). The relative standard deviation (RSD) for each dosage unit was calculated and the limit was set at 5%.

$$V_{\text{cylinder}} \text{ or } V_{\text{oblong}} = \frac{\pi \times d_1 \times d_2 \times h}{4} \quad (2)$$

$$V_{\text{heart}} = h \times \left[\pi \left(\frac{d_1}{1+\sin(45°)} \right)^2 + 4 \left(\frac{d_1}{1+\sin(45°)} \right)^2 \right] \quad (3)$$

2.8. Dissolution study

The *in vitro* dissolution study was conducted using an Xtend ™ apparatus (Sotax, Switzerland) for cylindrical, oblong and heart-shaped objects printed using the optimised formulation. Tablets (n = 6) were placed into baskets containing 900 mL of ultra-purified water at 37 °C and a stirring speed of 100 rpm. 3 mL samples were withdrawn through a 0.45 μm membrane filter at 0, 5, 10, 20, 30, 45 and 60 min. The calculation was corrected to take into account the volume withdrawn.

2.9. Data analysis

Built-in functions ("pca", "biplot", "corr", "clustergram", and "anovan") from MATLAB R2023a (MathWorks, USA) were utilised for data analysis. The rheological data were first mean-centred to remove any bias and then scaled to the variance of the dataset to ensure comparability. The "pca" function decomposed the data matrix into principal components (PCs), providing the factor loadings and observation scores. Following this, the "biplot" function was used to visualise the results, plotting both the matrix of factor loadings and the observation scores. The "corr" function was employed to build the correlation matrix of the dataset, and hierarchical clustering was performed using the "clustergram" function to group similar variables and reveal underlying patterns. Finally, analysis of variance (ANOVA) was conducted to identify significant factors at α = 5% using the "anovan" function.

3. Results and discussion

3.1. Evaluation of printability: manual vs. 3D printer

The printability (Pr) of these formulations was manually assessed as an initial step in the characterisation process to determine their suitability for extrusion-based printing. As shown in Fig. 1, formulations containing agar and HPMC exhibited Pr values between 0.9 and 1.1, and formulations containing sucrose and caffeine are not shown, as their Pr values also fell within this same range. In contrast, formulations containing only agar had Pr values exceeding 1.1.

The mean printability values, obtained from both the 3D printer and manual extrusion via syringe, are presented in Fig. 2. A comparison of the two techniques revealed that the mean printability values from the manual extrusion were higher than those from the 3D printer. Notably, the manual extrusion test did not effectively discriminate under-gelled samples (Pr < 0.94). This can likely be attributed to the larger syringe diameter (1.7 mm) compared to the 3D printer nozzle (0.8 mm), resulting in a lower pressure difference during extrusion, which made it less sensitive to under-gelled samples. However, this limitation is not of major concern, as under-gelled samples can still be printed with post-treatment if necessary. On the other hand, the

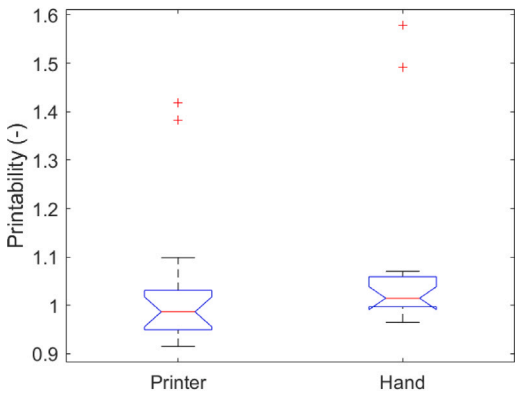

Fig. 2. Boxplot representation of the total mean values of the printability obtained from the 3D printer and manual extrusion.

manual test was successful in identifying over-gelled samples, which are unsuitable for printing. Furthermore, the difference between the two techniques was not statistically significant, as indicated by the p-value obtained from the Student's T-test (p = 0.4289). Based on these findings, the manual extrusion test was preferred over the 3D printer for identifying and excluding over-gelled samples.

The influence of each factor and their interactions on the printability of the formulations is illustrated in the Pareto chart (Fig. 3). Factors and interactions with a critical value exceeding 2.012 indicate statistically significant effects on printability ($p < 0.05$). Of these, the SSG concentration had the most significant impact. From the SSG effect plot, it is observed that an increase in SSG concentration led to a lower Pr (reflecting improved extrudability), as measured by the manual extrusion test. Similarly, the presence of HPMC was associated with a lower Pr, also suggesting enhanced extrudability. Interestingly, formulations with higher CP concentrations also demonstrated reduced Pr values, though this effect varied depending on the presence of HPMC or SSG and was not statistically significant (p >0.05). This observation is further highlighted by the significant interaction between HPMC and SSG, which underscores their combined effect on printability. To summarise, formulations lacking either HPMC or SSG achieved higher printability values. Conversely, formulations with 10% SSG and 2% HPMC had the lowest printability.

3.2. PCA analysis

Fig. 4 shows the biplot (loading and score plot) of the measured responses in space for the rheological parameters as obtained from the oscillatory measurement. Using Kaiser's rule, the first three components were kept since they had eigenvalues greater than 1.

PC 1 corresponded to 47.3% of the total sample variance and G', G'', CEM, δ, and m correlated positively with this axis whereas, γ_c correlated negatively. Regarding PC 2, δ, m, γ_c and τ_c correlated positively with this axis, explaining 27.8% of the sample's total variance. Notably, 0CP0SSG with the highest printability negatively correlated with this axis. For PC 3, δ and m correlated negatively with this axis whereas the rest correlated positively, explaining 16.7% of the total sample variance. Almost similar observations were observed in our previous studies (Aina et al., 2024c,a). Therefore, PC 1, PC 2 and PC 3 were attributed to the magnitude of force, the extrudability and the shape retention ability of the sample, respectively. This implies that, based on the rheological properties of the samples, specific formulations will exhibit optimal performance in different areas according to the PCs. For example, 2H10CP, with the highest correlation to PC 1, is expected to show the best extrudability. In contrast, 2H10SSG, correlating most strongly with PC 2, is anticipated to provide superior shape retention. Additionally, 2H10CP5SSG, with the highest correlation to PC 3, is projected to require the highest pressure for consistent extrusion.

3.3. Spearman's correlation test and hierarchical cluster analysis

The correlation test revealed statistically significant ($p < 0.05$) monotonic relationships between rheological parameters within the same groups, all showing positive correlations. As illustrated in Fig. 5, the hierarchical cluster analysis, complementing the correlation matrix, identified three main dendrograms corresponding to the previously identified PCs: extrusion force, extrudability, and shape retention.

The first dendrogram (in red) includes γ_c and τ_c, both of which describe the maximum strain and stress, respectively, that the material can withstand before deforming. These parameters are crucial as they indicate the force required to sustain the flow of the samples during printing, as well as the ease of flow through the nozzle. Higher values of γ_c and τ_c suggest that the material has a higher resistance to deformation for maintaining the printed shape, but also requires a higher extrusion force. The second main dendrogram (in green) includes m and δ. Both of these parameters provide insights into the viscoelastic behaviour of the material. Materials with low values of m and δ are more elastic and solid-like, exhibiting minimal deformation under stress, whereas materials with high values of m and δ are more viscous and liquid-like, flowing more easily. Thus, this dendrogram describes the homogeneity and stability of the extrusion process, with implications for the extrudability and precision of printed structures. The third dendrogram (in blue) is also related to elastic (G', CEM) and viscous behaviour (G''). Generally, materials with good shape retention possess high G'. Therefore, the third dendrogram consists of rheological parameters that describe the comportment after printing.

Gels with higher G' values tend to be more brittle, indicated by lower γ_c values (Anton Paar, 0000; Zhang et al., 2022). Consequently, it was not surprising to find a negative correlation between γ_c and G' ($p < 0.05$). In printability studies, it is important to recognise that while an increase in G' can improve shape retention, it may also result in increased brittleness, which can negatively impact extrudability. Regarding the correlation between the rheological parameters and the Pr values recorded, none showed significant correlations, in contrast to a prior study (Aina et al., 2024c). However, among all the rheological parameters, δ and m had the lowest p-value (0.15) and the highest (negative) correlations in the correlation matrix. This indicates that these parameters are the most indicative of printability (higher values associated with lower printability).

3.4. ANOVA analysis of factors and their interactions

Next, attempts were made to understand the influence of the main factors and their interactions on γ_c (representative of dendrogram 1), δ (representative of dendrogram 2), and G' (representative of dendrogram 3). The influence of each factor and their interactions on these parameters is shown in Fig. 6 where factors and interactions above the critical value of 2.101 indicate statistically significant influence ($p < 0.05$).

Fig. 6(a) shows that, excluding SSG, all factors and all three interactions significantly affected γ_c. Specifically, the addition of HPMC to the formulation leads to a notable increase in γ_c, suggesting that the formulation becomes less brittle. This observation aligns with previous studies (Aina et al., 2024c) and can be attributed to the formation of a less rigid network by HPMC at room temperature (Wang et al., 2021). Although this increased ductility improves the formulation's extrudability, it comes with the trade-off of requiring a higher extrusion force. In contrast, the addition of CP results in a significant decrease in γ_c, indicating increased brittleness. This brittleness is likely due to CP's ability to form a crosslinked network, resulting in a stiffer and more rigid structure that is more prone to fracture (Berardi et al., 2022; Drašković et al., 2020).

Conversely, Fig. 6(b) shows that only HPMC, SSG, and their interaction (H:SSG) significantly impact the phase angle (δ). The increase in δ upon the addition of HPMC confirms the presence of a less dense

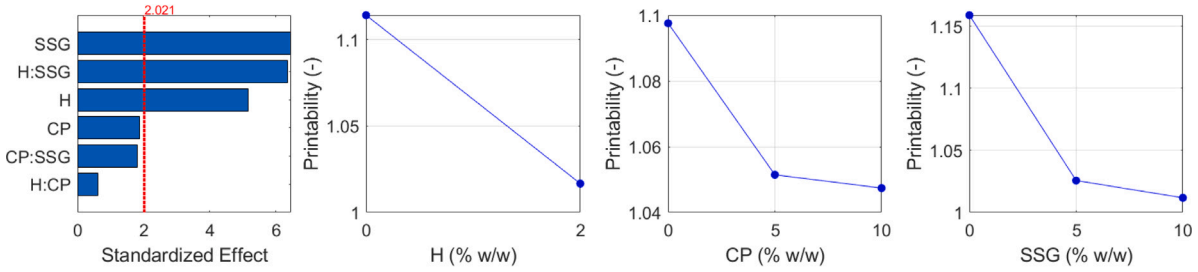

Fig. 3. Standardised effects of the factors on the printability of the samples.

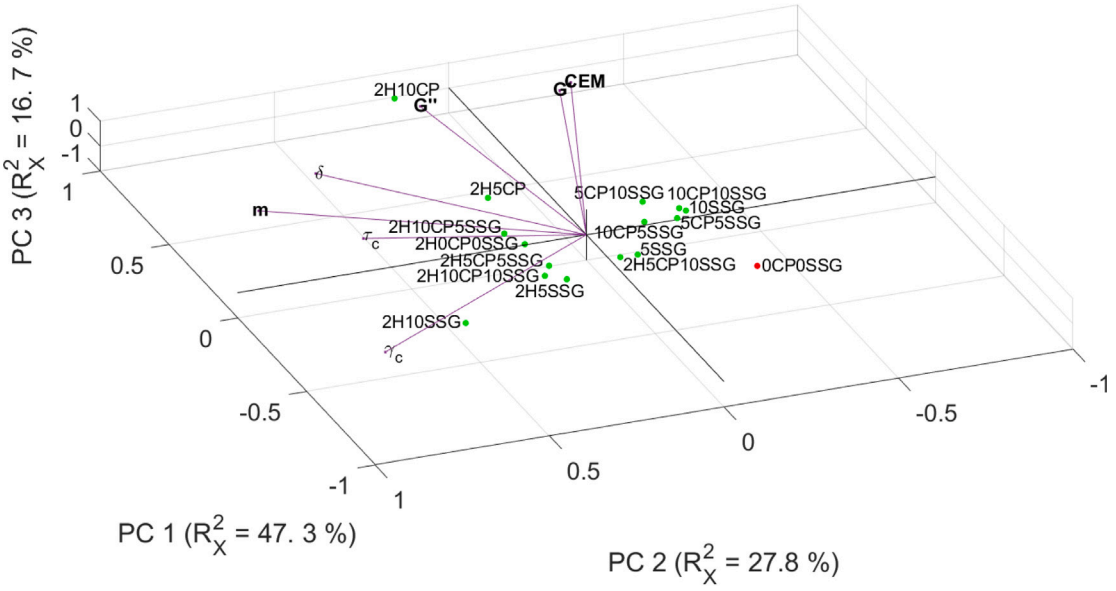

Fig. 4. PCA score and loading plot.
Coloured markers were based on the printability of the formulations: red: $Pr > 1.14$ and green: $0.94 < Pr < 1.14$.

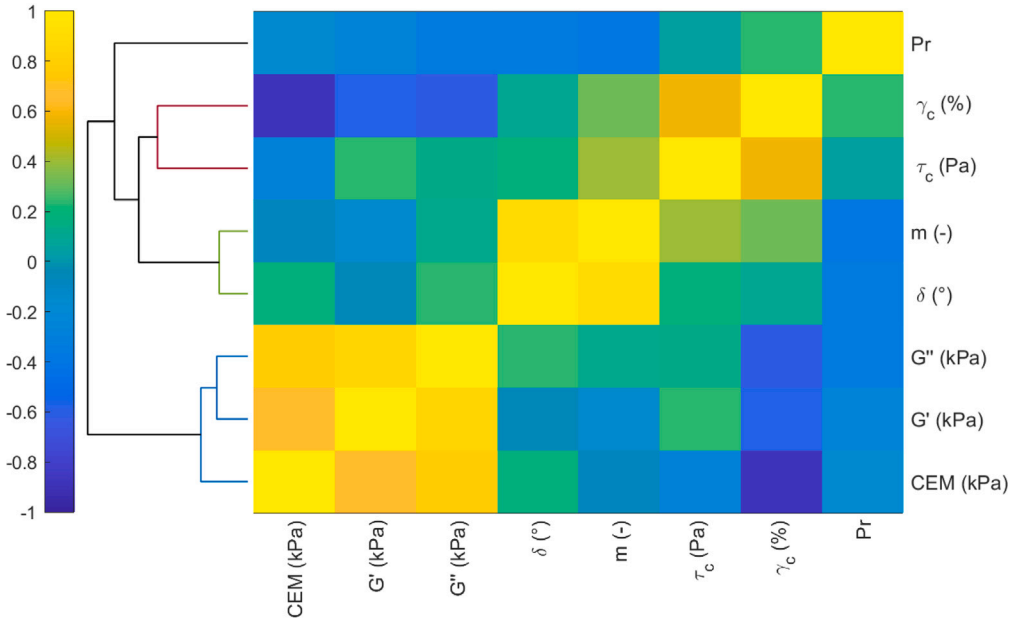

Fig. 5. Spearman rank-order correlation matrix and the linkage according to hierarchical cluster analysis of Spearman's correlations.

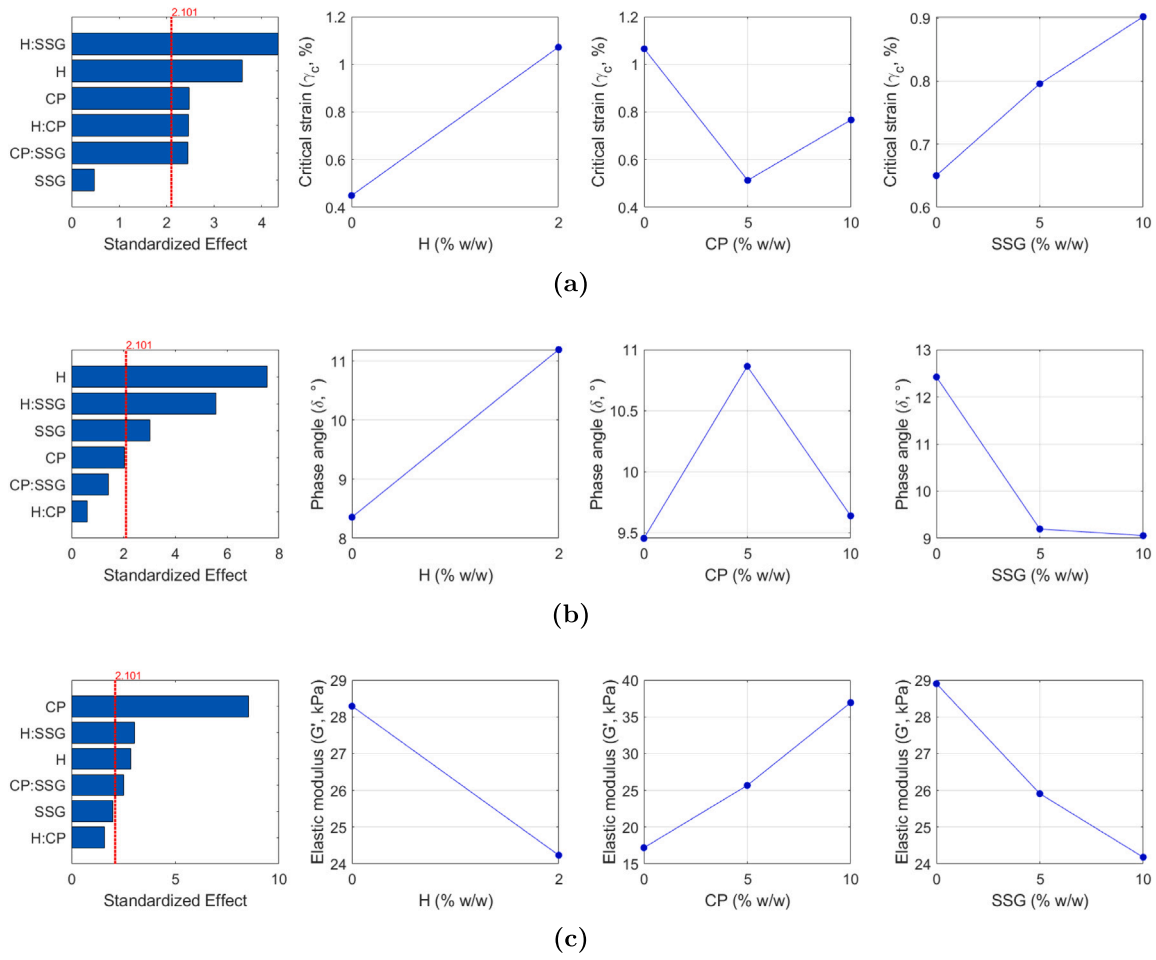

Fig. 6. Standardised effects of the factors on the critical strain (a), phase angle (b) and elastic modulus (c).

network, which translates to better extrudability, complementing its effect on γ_c. On the other hand, SSG primarily reduces δ, indicating a shift towards a more rigid gel structure. This effect is likely linked to SSG's ability to form gels upon hydration (Rojas et al., 2012; Soundaranathan et al., 2020; Comoglu and Bahadori, 2021), which increases elasticity. Consequently, formulations with high concentrations of SSG may exhibit poorer extrudability.

Fig. 6(c) demonstrates that CP, HPMC, and their interactions with SSG (H:SSG and CP:SSG) significantly influence the measured G'. CP notably increases G', suggesting improved shape retention and the formation of a more rigid network. However, this also results in poorer extrudability and higher extrusion force requirements. The increased G' due to CP is consistent with its role in forming a denser, crosslinked network, improving shape fidelity but at the cost of increased brittleness. In contrast, the addition of HPMC decreases G', aligning with earlier observations of enhanced ductility and reduced rigidity.

The interaction plots are illustrated in Fig. 7. Increasing SSG in formulations without HPMC generally decreased γ_c (Fig. 7(a)), increased δ (Fig. 7(b)), and increased G' (Fig. 7(c)). Conversely, in formulations containing HPMC, the addition of SSG results in the opposite effects—raising γ_c, lowering δ, and decreasing G'. Notably, when HPMC is combined with 10 % SSG, it only produces a 2% increase in δ, compared to the 20% increase with 5% SSG. This reduction can be attributed to SSG's formation of a rigid gel network, which limits polymer chain mobility and diminishes the benefits of HPMC in enhancing extrudability (Soundaranathan et al., 2020; Drašković et al., 2020).

CP also adds complexity to the interactions between factors. Incorporating CP into the formulation leads to the formation of a dense network structure within the polymer matrix. This network formation results in decreased chain mobility, as evidenced by the overall reduction in γ_c (Figs. 7(d) and 7(e)) and an increase in G' (Fig. 7(f)), as the concentration of CP increases in the formulations. Although these observations could enhance the rigidity and shape retention of the formulation, they also contribute to increased brittleness and poorer extrudability.

In summary, formulations containing HPMC exhibit better extrudability but require higher extrusion forces and show lower shape retention. CP improves shape retention but decreases extrudability. SSG negatively impacts both extrudability and shape retention. The interaction of these factors adds complexity, highlighting the need for a nuanced balance to optimise formulation properties. As a result, formulations such as 0CP0SSG, 5CP0SSG, 10CP0SSG, and 2H10CP0SSG were excluded from further evaluation due to their suboptimal performance in terms of extrudability, shape retention, and rigidity.

3.5. Disintegration time

Out of the 14 formulations tested, only 5 successfully disintegrated. These formulations and their respective disintegration times were as follows: 0CP5SSG (1.27 ± 0.04 s), 0CP10SSG (0.38 ± 0.04 s), 5CP5SSG (0.46 ± 0.03 s), 5CP10SSG (0.91 ± 0.28 s), and 10CP5SSG (1.30 ± 0.11 s). Formulations containing 5% and 10% sodium starch glycolate (SSG) disintegrated effectively, with faster disintegration observed at higher SSG concentrations. However, an unexpected trend emerged in formulations containing both crospovidone (CP) and SSG. Increasing the concentration of either disintegrant led to slower disintegration times. This behaviour can be attributed to the simultaneous presence of CP and SSG, which resulted in the formation of a denser gel-like barrier

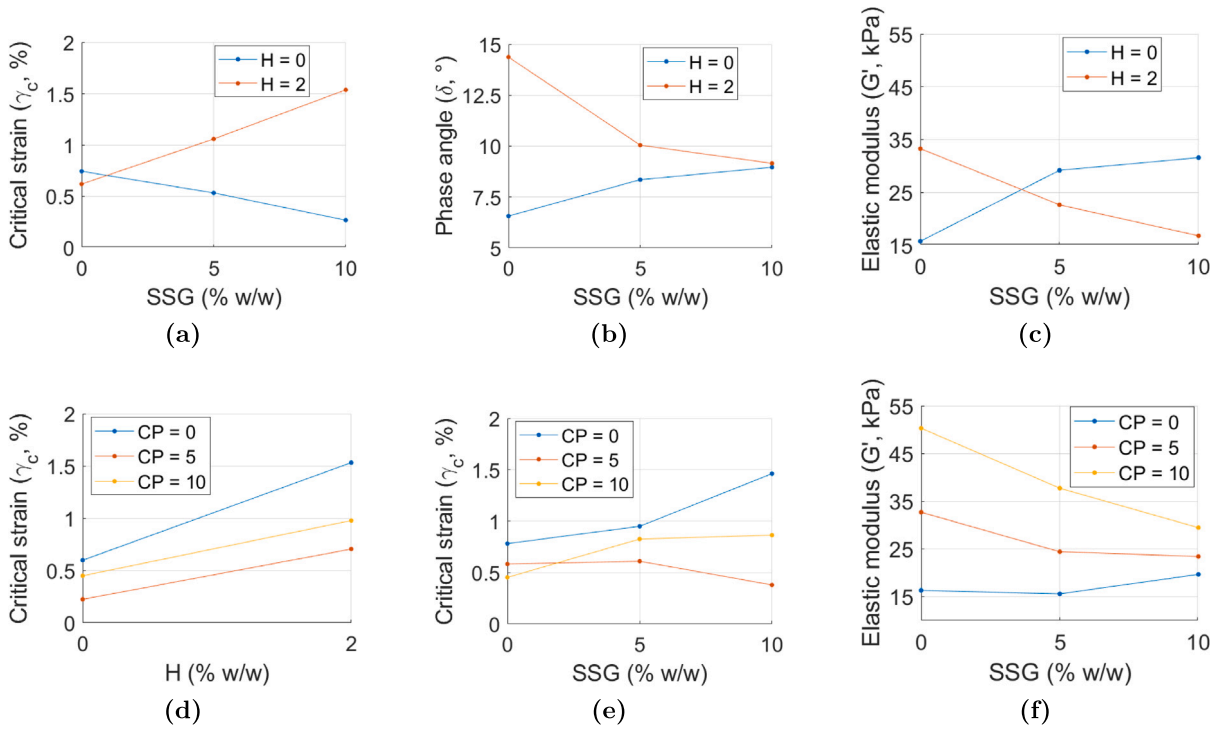

Fig. 7. Interaction plot of HPMC:SSG on the critical strain (a), HPMC:SSG on the phase angle (b), HPMC:SSG on the elastic modulus (c), CP:HPMC on the critical strain (d), CP:SSG on the critical strain and CP:SSG on the elastic modulus (f).

that impedes water penetration, ultimately delaying the disintegration process (Desai et al., 2014).

Similarly, formulations containing HPMC failed to disintegrate, likely due to the formation of a gel layer upon contact with water. This observation aligns with our previous study (Aina et al., 2024b), where it was observed that samples with a higher surface area to volume ratio (SA/V) disintegrated faster (within 180 s), while samples with masses greater than 1.2 g and a lower SA/V ratio exhibited disintegration times longer than 180 s. The thicker gel layer formed in the larger samples may also contribute to hindering the disintegration. Together, these findings suggest that both formulation composition and physical characteristics, such as SA/V, play a significant role in the disintegration process.

Although 0CP10SSG exhibited the fastest disintegration time and might initially appear to be the optimal formulation based solely on this criterion, a comparison of its rheological properties with those of 10S2C—the optimal formulation identified in our previous work (Aina et al., 2024c)—revealed that 5CP10SSG more closely resembles 10S2C. This suggests that 5CP10SSG strikes a more favourable balance between rapid disintegration and desirable rheological properties. Consequently, 5CP10SSG was selected for printing.

3.6. Printing process

As shown in Fig. 8(a), the printed objects were white and while soft to touch, they can be readily manipulated. However, a significant challenge arose due to the lower water content in the 5CP10SSG formulation. This reduction in water content caused the caffeine to recrystallise upon drying, as shown in Fig. 8(b). Nevertheless, for this study, the drying of the object was not desired, therefore, the recrystallisation of caffeine was minimised.

Although the printed objects suffered from poor resolution, similar to those produced in Aina et al. (2024b), overall better results were achieved. This improvement could be due to the slightly lower Pr of 5CP10SSG compared to 10S2C (2H0CP0SSG). The difference in printability between the two formulations was further highlighted when comparing the regression fit of the printed objects' volume to the geometric volume of the models. As shown in Fig. 9(a), the slope for 10S2C deviated more from 1 than that for 5CP10SSG, indicating greater discrepancy between the intended and actual printed volumes for 10S2C. Interestingly, the slopes describing the mass and volume of printed objects were similar for both formulations (Fig. 9(b)). Moreover, combining both datasets resulted in an R^2 >0.99. This suggests that using the same printing parameters such as speed, geometry, and infill density, printed objects presenting similar mass and dosage, should be obtained. However, the actual volume of the printed object and its deviation from the model's volume would depend on the formulation's printability (i.e., shape retention and extrudability).

As shown in Table 5, the models accurately predicted the mass of the printed objects based on their specified dimensions, with all measured values falling within the predicted confidence intervals. This confirms the reliability of the approach and demonstrates its potential to enhance the precision of 3D-printed pharmaceuticals. Consequently, these predictive models could greatly optimise dose personalisation and ensure consistency in the printing process, reducing variability associated with manual adjustments. While further studies are needed to establish a direct correlation between drug content and measured mass, it is estimated that 1 gram of the printing formulation would contain approximately 20 mg of caffeine which corresponds to 2% contained in the formulation. This indicates that the approach is scalable and adaptable for various formulations and APIs. Therefore, predicting mass from geometric dimensions provides a robust foundation for dosage personalisation, especially for complex dosage forms or formulations with narrow therapeutic indices. Incorporating this data collection method into the 3D printer's verification and validation process could reduce the trial-and-error typically associated with 3D printing, leading to more efficient production cycles and consistent product quality. Additionally, these models simplify the estimation of dimensions needed to achieve the desired drug content, enabling precise tailoring of drug dosages for individual patients. This improves medication management and offers greater accuracy than traditional compounding methods.

Fig. 8. Bunny and IMT logo printed using 5CP10SSG formulation (a), and bunny left at room temperature overnight (b).

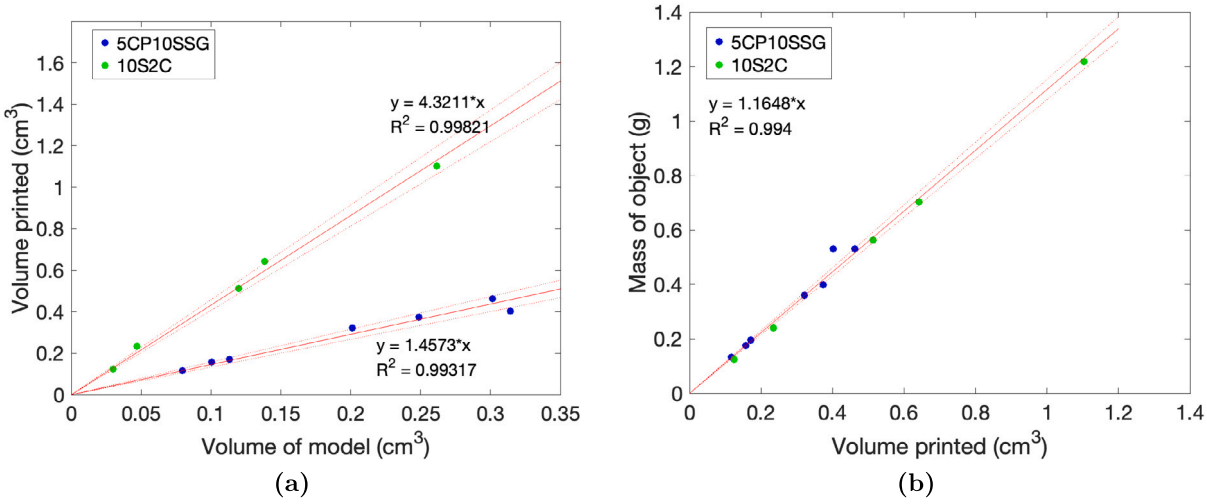

Fig. 9. Linear relationship between the theoretical volume and experimental volume (a). Linear relationship between the experimental volume and mass of printed objects (b).

Table 5
Predicted mass of various shapes from the geometric volumes of the model.

Shape	Volume (cm^3)		Mass (g)	
	Geometric	Pycnometric	Measured (range)	Predicted (95% CI)
Cylinder	0.079	0.116	0.127 – 0.138	0.124 – 0.145
Heart	0.424	0.548	0.686 – 0.705	0.663 – 0.775
Oblong	0.226	0.332	0.354 – 0.361	0.354 – 0.414

3.7. Dissolution study

As shown in Fig. 10, the three shapes (cylinder, heart, and oblong) printed using the optimised formulation 5CP10SSG demonstrated immediate release properties, with over 80% of caffeine released within the first 45 min. Although the final caffeine concentration from the oblong shape varied between approximately 80% and 86%, its dissolution profile remained comparable to that of the other shapes. Although all shapes exhibited complete drug release within 10 min, the dissolution curves were extended to 60 min to ensure stable and complete release, thereby allowing the observation of any potential re-adsorption or instability effects (Almáši et al., 2020; Dara et al., 2019). This extended data also provides a more comprehensive understanding of the release profile and serves as a foundation for future comparisons with other formulations.

Importantly, the consistent performance observed across different shapes demonstrates that the disintegration properties of the optimised formulation are robust and largely unaffected by geometric variations. This indicates that the formulation itself is the primary determinant of both disintegration and release characteristics, rather than the geometry of the printed objects. These findings stand in contrast to those of a previous study (Aina et al., 2024b), where the dissolution behaviour was found to be significantly influenced by physical properties, such as the SA/V of the printed shapes. By showing that formulation is the key driver of disintegration, our study highlights the potential for more predictable and uniform behaviour across a range of printed geometries. This offers the flexibility to customise dosage forms without sacrificing effectiveness. Moving forward, it will be crucial to address potential batch-to-batch variability to ensure consistent results across production runs. Additionally, evaluating the long-term stability of the dosage form will be essential to confirm its reliability and sustained effectiveness in practical applications.

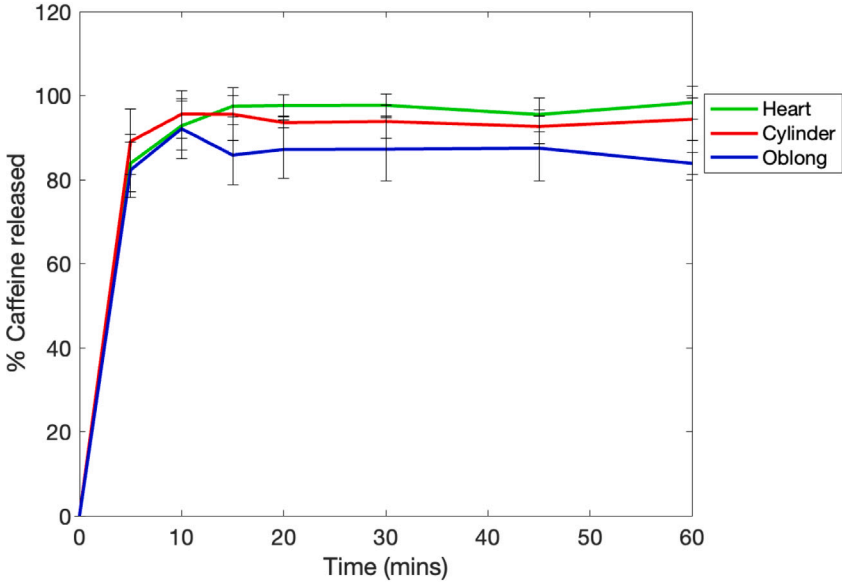

Fig. 10. Dissolution curve of printed objects of various shapes.

4. Conclusion

This study explored the effects of hydroxypropyl methylcellulose (HPMC), sodium starch glycolate (SSG), and crospovidone (CP) on the printability, disintegration time, and rheological properties of hydrogel formulations intended for semi-solid extrusion (SSE). Based on our hypothesis, formulations with rheological properties similar to a previously optimised formulation were expected to exhibit also optimal printability, and that the inclusion of CP and SSG would enhance disintegration and accelerate immediate-release properties. And indeed, it was found that the incorporation of CP and SSG significantly improved the disintegration properties of the formulations. Specifically, the formulation containing both CP and SSG demonstrated enhanced disintegration and faster release rates compared to formulations without these excipients. In addition, the rheological properties were categorised based on factors that influence printability: extrudability, shape retention, and extrusion force. Our findings revealed that while HPMC significantly enhanced extrudability, it had limited effects on shape retention and disintegration. In contrast, CP improved shape retention and structural integrity, but at the cost of reduced extrudability and increased extrusion force due to its higher elastic modulus. The inclusion of SSG mitigated these limitations, resulting in improved overall printability. The optimal formulation, consisting of 5% CP and 10% SSG, exhibited favourable rheological properties to be used for SSE 3D printing and aligned with those of the previously developed formulation. This led to effective disintegration as well as improved printability, ensuring the formulation was capable of rapid drug release. Furthermore, linear regression analysis of the volume of the model versus the printed objects showed minimal deviation (with a slope close to 1), underscoring the potential for consistent and reproducible performance across production batches. While all formulations demonstrated immediate-release properties, the flexibility of 3D printing broadens the potential for personalised dosage applications, especially in situations requiring rapid drug release. These findings suggest that straightforward characterisation methods can be employed to develop extrusion-compatible formulations, supporting the creation of tailored drug delivery systems with high precision. In conclusion, this study demonstrates that incorporating CP and SSG into hydrogel formulations for SSE 3D printing significantly enhances disintegration and printability, achieving high precision in dosage form development. Although further studies on scalability, long-term stability, and additional optimisation are necessary, these results provide a promising foundation for developing personalised, fast-disintegrating drug delivery systems using 3D printing.

CRediT authorship contribution statement

Morenikeji Aina: Writing – original draft, Visualization, Methodology, Investigation, Data curation, Conceptualization. **Darya Kuznyetsova:** Investigation, Data curation. **Fabien Baillon:** Writing – review & editing, Visualization, Software. **Romain Sescousse:** Writing – review & editing, Supervision. **Noelia M. Sanchez-Ballester:** Writing – review & editing, Methodology, Conceptualization. **Sylvie Begu:** Writing – review & editing, Supervision, Project administration. **Ian Soulairol:** Writing – review & editing, Validation, Supervision, Methodology, Conceptualization. **Martial Sauceau:** Writing – review & editing, Validation, Supervision, Resources, Methodology, Funding acquisition, Conceptualization.

Funding

The authors are grateful to the Occitanie Region, France and ANR "Investissements d'Avenir" program, France for their financial support under grant number ANR-18-EURE-0021.

Declaration of competing interest

The authors declare that they have no known competing financial interests or personal relationships that could have appeared to influence the work reported in this paper.

Data availability

The rheological data for formulations containing disintegrants is available here: Recherche Data Gouv.

References

Abdella, S., Kim, S., Afinjuomo, F., Song, Y., Upton, R., Garg, S., 2024. Combining the potential of 3D printed buccal films and nanostructured lipid carriers for personalised cannabidiol delivery. Drug Deliv. Transl. Res. 14 (4), 984–1004. http://dx.doi.org/10.1007/s13346-023-01446-0.

Aina, M., Baillon, F., Sescousse, R., Sanchez-Ballester, N.M., Begu, S., Soulairol, I., Sauceau, M., 2024a. Assessing texturometer-derived rheological data for predicting the printability of gummy formulations in SSE 3D printing. Int. J. Pharm. 662, 124471. http://dx.doi.org/10.1016/j.ijpharm.2024.124471.

Aina, M., Baillon, F., Sescousse, R., Sanchez-Ballester, N.M., Begu, S., Soulairol, I., Sauceau, M., 2024b. Development of personalised immediate-release gel-based formulations using semi-solid extrusion. Gels 10 (10), 665. http://dx.doi.org/10.3390/gels10100665.

Aina, M., Baillon, F., Sescousse, R., Sanchez-ballester, N.M., Begu, S., Soulairol, I., Sauceau, M., 2024c. Evaluation of the printability of agar and hydroxypropyl methylcellulose gels as gummy formulations: insights from rheological properties. Int. J. Pharm. 654, 123937. http://dx.doi.org/10.1016/j.ijpharm.2024.123937.

Almáši, M., Beňová, E., Zeleňák, V., Madaj, B., Huntošová, V., Brus, J., Urbanová, M., Bednarčík, J., Hornebecq, V., 2020. Cytotoxicity study and influence of SBA-15 surface polarity and pH on adsorption and release properties of anticancer agent pemetrexed. Mater. Sci. Eng.: C 109, 110552. http://dx.doi.org/10.1016/j.msec.2019.110552.

Anton Paar, A.P., 0000. Amplitude sweeps, https://wiki.anton-paar.com/en/amplitude-sweeps/.

Awad, A., Trenfield, S.J., Basit, A.W., 2021. Chapter 19 - solid oral dosage forms. In: Adejare, A. (Ed.), Remington (Twenty-Third Edition). Academic Press, pp. 333–358. http://dx.doi.org/10.1016/B978-0-12-820007-0.00019-2.

Baral, K.C., Bajracharya, R., Lee, S.H., Han, H.K., 2021. Advancements in the pharmaceutical applications of probiotics: dosage forms and formulation technology. Int. J. Nanomedicine Volume 16, 7535–7556. http://dx.doi.org/10.2147/IJN.S337427.

Berardi, A., Bisharat, L., Quodbach, J., Abdel Rahim, S., Perinelli, D.R., Cespi, M., 2021. Advancing the understanding of the tablet disintegration phenomenon – An update on recent studies. Int. J. Pharm. 598, 120390. http://dx.doi.org/10.1016/j.ijpharm.2021.120390.

Berardi, A., Janssen, P.H.M., Dickhoff, B.H.J., 2022. Technical insight into potential functional-related characteristics (FRCs) of sodium starch glycolate, croscarmellose sodium and crospovidone. J. Drug Deliv. Sci. Technol. 70, 103261. http://dx.doi.org/10.1016/j.jddst.2022.103261.

Bowler, A.L., Bakalis, S., Watson, N.J., 2020. A review of in-line and on-line measurement techniques to monitor industrial mixing processes. Chem. Eng. Res. Des. 153, 463–495. http://dx.doi.org/10.1016/j.cherd.2019.10.045.

Comoglu, T., Bahadori, F., 2021. Granulation and production approaches of orally disintegrating tablets. In: Handbook of Pharmaceutical Granulation Technology, fourth ed. CRC Press, pp. 556–571.

Dara, T., Vatanara, A., Nabi Meybodi, M., Vakilinezhad, M.A., Malvajerd, S.S., Vakhshiteh, F., Shamsian, A., Sharifzadeh, M., Kaghazian, H., Mosaddegh, M.H., 2019. Erythropoietin-loaded solid lipid nanoparticles: preparation, optimization, and in vivo evaluation. Colloids Surf. B 178, 307–316. http://dx.doi.org/10.1016/j.colsurfb.2019.01.027.

Deon, M., dos Santos, J., de Andrade, D.F., Beck, R.C.R., 2022. A critical review of traditional and advanced characterisation tools to drive formulators towards the rational development of 3D printed oral dosage forms. Int. J. Pharm. 628, 122293. http://dx.doi.org/10.1016/j.ijpharm.2022.122293.

Desai, P.M., Er, P.X.H., Liew, C.V., Heng, P.W.S., 2014. Functionality of disintegrants and their mixtures in enabling fast disintegration of tablets by a quality by design approach. AAPS PharmSciTech 15 (5), 1093–1104. http://dx.doi.org/10.1208/s12249-014-0137-4.

Drašković, M., Turković, E., Vasiljević, I., Trifković, K., Cvijić, S., Vasiljević, D., Parojčić, J., 2020. Comprehensive evaluation of formulation factors affecting critical quality attributes of casted orally disintegrating films. J. Drug Deliv. Sci. Technol. 56, 101614. http://dx.doi.org/10.1016/j.jddst.2020.101614.

El Aita, I., Rahman, J., Breitkreutz, J., Quodbach, J., 2020. 3D-printing with precise layer-wise dose adjustments for paediatric use via pressure-assisted microsyringe printing. Eur. J. Pharmaceut. Biopharmaceut. 157, 59–65. http://dx.doi.org/10.1016/j.ejpb.2020.09.012.

Funk, N.L., Fantaus, S., Beck, R.C.R., 2022. Immediate release 3D printed oral dosage forms: how different polymers have been explored to reach suitable drug release behaviour. Int. J. Pharm. 625, 122066. http://dx.doi.org/10.1016/j.ijpharm.2022.122066.

Herrada-Manchón, H., Rodríguez-González, D., Alejandro Fernández, M., Suñé-Pou, M., Pérez-Lozano, P., García-Montoya, E., Aguilar, E., 2020. 3D printed gummies: personalized drug dosage in a safe and appealing way. Int. J. Pharm. 587, http://dx.doi.org/10.1016/j.ijpharm.2020.119687.

Kokott, M., Lura, A., Breitkreutz, J., Wiedey, R., 2021. Evaluation of two novel co-processed excipients for direct compression of orodispersible tablets and mini-tablets. Eur. J. Pharmaceut. Biopharmaceut. 168, 122–130. http://dx.doi.org/10.1016/j.ejpb.2021.08.016.

Liang, K., Brambilla, D., Leroux, J.C., 2019. Is 3D printing of pharmaceuticals a disruptor or enabler? Adv. Mater. 31 (5), 1805680. http://dx.doi.org/10.1002/adma.201805680.

Ouyang, L., Yao, R., Zhao, Y., Sun, W., 2016. Effect of bioink properties on printability and cell viability for 3D bioplotting of embryonic stem cells. Biofabrication 8 (3), 035020. http://dx.doi.org/10.1088/1758-5090/8/3/035020.

Panraksa, P., Zhang, B., Rachtanapun, P., Jantanasakulwong, K., Qi, S., Jantrawut, P., 2022. 'Tablet-in-syringe': A novel dosing mechanism for dysphagic patients containing fast-disintegrating tablets fabricated using semisolid extrusion 3D printing. Pharmaceutics 14 (2), 443. http://dx.doi.org/10.3390/pharmaceutics14020443.

Patel, S.K., Khoder, M., Peak, M., Alhnan, M.A., 2021. Controlling drug release with additive manufacturing-based solutions. Adv. Drug Deliv. Rev. 174, 369–386. http://dx.doi.org/10.1016/j.addr.2021.04.020.

Roche, A., Sanchez-Ballester, N.M., Aubert, A., Rossi, J.-C., Begu, S., Soulairol, I., 2023. Preliminary study on the development of caffeine oral solid form 3D printed by semi-solid extrusion for application in neonates. AAPS PharmSciTech 24 (122), http://dx.doi.org/10.1208/s12249-023-02582-z.

Rojas, J., Guisao, S., Ruge, V., 2012. Functional assessment of four types of disintegrants and their effect on the spironolactone release properties. AAPS PharmSciTech 13 (4), 1054–1062. http://dx.doi.org/10.1208/s12249-012-9835-y.

Rosas, J.G., Brush, P., Thompson, B., Miller, C., Overton, P., Tugby, N., Stoliarskaia, D., Hurley, S., Ramasamy, M., Conway, S.L., 2023. Implementation of a fully integrated CM direct compression and coating process at a commercial pharmaceutical facility – Part 2: PAT and RTD results for normal operational conditions batches. Int. J. Pharm. 636, 122814. http://dx.doi.org/10.1016/j.ijpharm.2023.122814.

Schick, P., Sager, M., Voelker, M., Weitschies, W., Koziolek, M., 2020. Application of the GastroDuo to study the interplay of drug release and gastric emptying in case of immediate release aspirin formulations. Eur. J. Pharmaceut. Biopharmaceut. 151, 9–17. http://dx.doi.org/10.1016/j.ejpb.2020.03.013.

Sohail Arshad, M., Zafar, S., Yousef, B., Alyassin, Y., Ali, R., AlAsiri, A., Chang, M.W., Ahmad, Z., Ali Elkordy, A., Faheem, A., Pitt, K., 2021. A review of emerging technologies enabling improved solid oral dosage form manufacturing and processing. Adv. Drug Deliv. Rev. 178, 113840. http://dx.doi.org/10.1016/j.addr.2021.113840.

Soundaranathan, M., Vivattanaseth, P., Walsh, E., Pitt, K., Johnston, B., Markl, D., 2020. Quantification of swelling characteristics of pharmaceutical particles. Int. J. Pharm. 590, 119903. http://dx.doi.org/10.1016/j.ijpharm.2020.119903.

Steffens, K.E., Wagner, K.G., 2021. Immediate-release formulations produced via twin-screw melt granulation: systematic evaluation of the addition of disintegrants. AAPS PharmSciTech 22 (5), 183. http://dx.doi.org/10.1208/s12249-021-02056-0.

Stranzinger, S., Markl, D., Khinast, J.G., Paudel, A., 2021. Review of sensing technologies for measuring powder density variations during pharmaceutical solid dosage form manufacturing. TRAC Trends Anal. Chem. 135, 116147. http://dx.doi.org/10.1016/j.trac.2020.116147.

Tagami, T., Ito, E., Kida, R., Hirose, K., Noda, T., Ozeki, T., 2021. 3D printing of gummy drug formulations composed of gelatin and an HPMC-based hydrogel for pediatric use. Int. J. Pharm. 594, http://dx.doi.org/10.1016/j.ijpharm.2020.120118.

Trisopon, K., Kittipongpatana, N., Kittipongpatana, O.S., 2020. A spray-dried, co-processed rice starch as a multifunctional excipient for direct compression. Pharmaceutics 12 (6), 518. http://dx.doi.org/10.3390/pharmaceutics12060518.

Trisopon, K., Kittipongpatana, N., Wattanaarsakit, P., Kittipongpatana, O.S., 2021. Formulation study of a co-processed, rice starch-based, all-in-one excipient for direct compression using the sedem-odt expert system. Pharmaceuticals 14 (10), 1047. http://dx.doi.org/10.3390/ph14101047.

Wang, N., Shi, H., Yang, S., 2022. 3D printed oral solid dosage form: modified release and improved solubility. J. Control. Release 351, 407–431. http://dx.doi.org/10.1016/j.jconrel.2022.09.023.

Wang, Y., Yu, L., Sun, Q., Xie, F., 2021. Hydroxypropyl methylcellulose and hydroxypropyl starch: rheological and gelation effects on the phase structure of their mixed hydrocolloid system. Food Hydrocolloids 115, 106598. http://dx.doi.org/10.1016/j.foodhyd.2021.106598.

Wilkins, C.A., Hamman, H., Hamman, J.H., Steenekamp, J.H., 2024. Fixed-dose combination formulations in solid oral drug therapy: advantages, limitations, and design features. Pharmaceutics 16 (2), 178. http://dx.doi.org/10.3390/pharmaceutics16020178.

Xue, A., Li, W., Tian, W., Zheng, M., Shen, L., Hong, Y., 2023. A bibliometric analysis of 3D printing in personalized medicine research from 2012 to 2022. Pharmaceuticals 16 (11), 1521. http://dx.doi.org/10.3390/ph16111521.

Zarmpi, P., Flanagan, T., Meehan, E., Mann, J., Fotaki, N., 2017. Biopharmaceutical aspects and implications of excipient variability in drug product performance. Eur. J. Pharmaceut. Biopharmaceut. 111, 1–15. http://dx.doi.org/10.1016/j.ejpb.2016.11.004.

Zhang, J., Vo, A.Q., Feng, X., Bandari, S., Repka, M.A., 2018. Pharmaceutical additive manufacturing: A novel tool for complex and personalized drug delivery systems. AAPS PharmSciTech 19 (8), 3388–3402. http://dx.doi.org/10.1208/s12249-018-1097-x.

Zhang, Y., Wang, Y., Zhang, R., Yu, J., Gao, Y., Mao, L., 2022. Tuning the rheological and tribological properties to simulate oral processing of novel high internal phase oleogel-in-water emulsions. Food Hydrocolloids 131, 107757. http://dx.doi.org/10.1016/j.foodhyd.2022.107757.